1. Baseline Predictions for Open and Hidden Heavy Flavor Production at RHIC II

Ramona Vogt, LBNL and UC Davis

Charm and bottom hadrons can be detected two ways. The reconstruction of charm through charged hadron decays such as $D^0 \to K^-\pi^+$ (3.8%) and $D^+ \to K^-\pi^+\pi^+$ (9.1%) gives the full momentum of the initial D meson, yielding the best direct measurement. The B meson decay channels, with the exception of $B^\pm \to J/\psi K^\pm$, involve more particles. In addition, the branching ratios are all smaller – the $J/\psi K$ decay channel has a branching ratio of 0.1%. Heavy flavors can also be detected indirectly via semi-leptonic decays such as $D \to lX$, $B \to lX$ and $B \to DX \to lX'$ although the momentum of the parent heavy flavor hadron remains unknown. Early measurements of prompt leptons in beam dump experiments assumed that the density of the dump was high enough to absorb semi-leptonic decays of non-charm hadrons, leaving only the charm component. At modern colliders, it is not possible to use beam dumps to measure charm from leptons but, at sufficiently high p_T, electrons from heavy flavor decays emerge from hadronic cocktails.

To separate D and B decays to leptons, the cross sections need to be accurately measured. The total cross sections are very sensitive to the renormalization μ_R, and factorization, μ_F, scales and the heavy quark mass, m_Q. This is especially true for charm since m_c is close to the minimum scale of the parton densities, $\mu_{\rm min}$. In the case of the CTEQ6M densities, backwards evolution to scales below $\mu_{\rm min}$ causes the gluon distribution to decrease at low x and, at low μ, become zero since $xg(x,\mu^2) \equiv 0$ if the evolution would result in a negative gluon density. Therefore past fits of m and μ assume $\mu_R = \mu_F \geq \mu_{\rm min}$. For charm quarks this essentially requires $\mu \geq m_c$ with best agreement being found for $\mu = 2m_c$ and $m_c = 1.2$ GeV. For these values, the total cross section is well behaved as the collision energy increases, as shown on the left-hand side of Fig. 1. Instead of trying to produce a "best fit" at fixed-target energies and extrapolating the fit to higher energies, another approach, as used recently in Ref. [1], is to define an uncertainty band within $1.3 < m_c < 1.7$ GeV with $(\mu_F/m_c, \mu_R/m_c) = (1,1)$, (2,2), (0.5,0.5), (0.5,1), (1,0.5), (1,2), (2,1). The resulting $c\overline{c}$ total cross sections are shown on the right-hand side of Fig. 1. Note that for the cases where $\mu_F/m_c = 0.5$, the cross sections flatten with energy instead of continuing to increase steadily due to phase space, as do the calculations with the higher values of μ_F/m_c. The K factors, on the other hand, are largest for the cases where $\mu_R/m_c = 0.5$ since $\alpha_s(0.5m_c) = 0.625$. Results for bottom production are less problematic since the quark mass is several times larger than the charm quark mass.

We now turn to predictions of the transverse momentum, p_T, distributions of charm and bottom quarks as well as the charm and bottom hadron distributions resulting from fragmentation, see Ref. [1] for details and a list of references. Theoretical uncertainties due to the mass and scale choice are estimated. Our final prediction is thus not a single curve but rather an uncertainty band which has a reasonably large probability of containing the 'true' theoretical prediction. The lower scales present less of a problem for the p_T distributions than for the total cross sections since the scale is proportional to m_T rather than m_Q and the growth of α_s for the lowest scales is tamed for p_T's of 2-3 GeV.

The Lorentz-invariant distribution, $Ed^3\sigma(Q)/dp_Q^3$, is evaluated at Fixed-Order Next-to-Leading Logarithm (FONLL). In addition to including the full fixed-order NLO result, the FONLL calculation also resums large perturbative terms proportional to $\alpha_s^n \log^k(p_T/m_Q)$ to all orders with next-to-leading logarithmic (NLL) accuracy (i.e. $k = n, n-1$) where m_Q is the heavy quark mass. The perturbative parameters are the heavy quark mass and the value of the strong coupling, α_s. We take $m_c = 1.5$ GeV and $m_b = 4.75$ GeV as central values and vary the masses over the range $1.3 < m_c < 1.7$ GeV for charm and $4.5 < m_b < 5$ GeV for bottom to estimate the mass uncertainties. We set the 5 flavor QCD scale to the value of the CTEQ6M parton densities, $\Lambda^{(5)} = 0.226$ GeV. The sensitivity of the cross section to the scale can be used to estimate the uncertainty due to the absence of higher orders. We have taken $\mu_{R,F} = \mu_0 = \sqrt{p_T^2 + m^2}$ as the central value and varied the two scales independently within a 'fiducial' region defined by $0.5 \leq \mu_{R,F}/\mu_0 \leq 2$ and $0.5 \leq \mu_R/\mu_F \leq 2$. In practice, we use the following seven

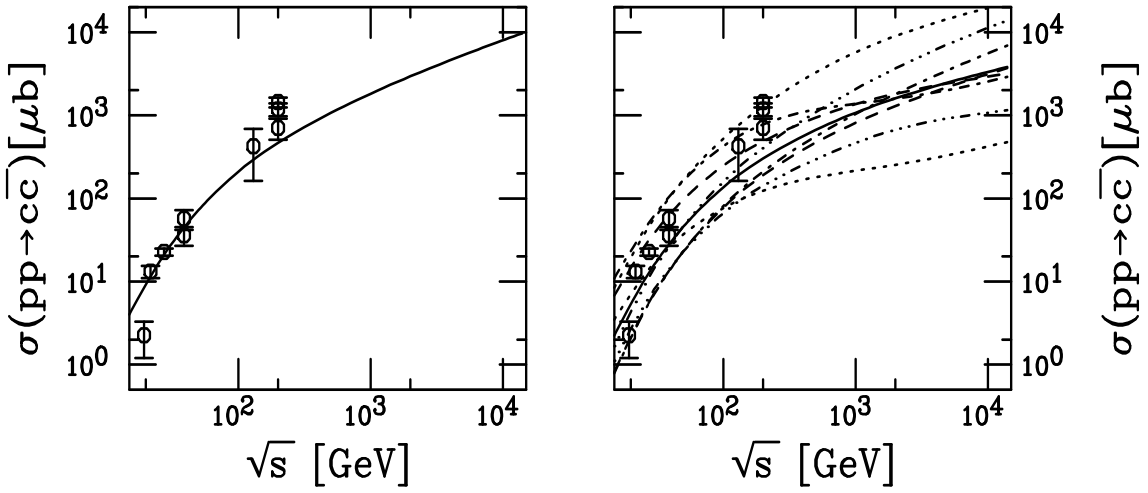

Fig. 1: Total $c\bar{c}$ cross sections calculated using CTEQ6M. Left-hand side: A "fit" of the lower energy data with $m_c = 1.2$ GeV and $\mu = 2m_c$. Right-hand side: The "fiducial" range of the theoretical uncertainty. The solid curve is the central value $(\mu_F/m_c, \mu_R/m_c) = (1,1)$ with $m_c = 1.5$ GeV. The upper and lower dashed curves are $m_c = 1.3$ and 1.7 GeV with (1,1) respectively. The upper and lower dot-dashed curves correspond to (0.5,0.5) and (2,2) while the upper and lower dotted curves are with (1,0.5) and (0.5,1) with $m = 1.5$ GeV and the upper and lower dot-dot-dot dashed curves employ (2,1) and (1,2).

sets: $(\mu_R/\mu_0, \mu_F/\mu_0) = (1,1)$, (2,2), (0.5,0.5), (1,0.5), (2,1), (0.5,1), (1,2). The envelope containing the resulting curves defines the uncertainty. Finally, the uncertainties stemming from mass and scale variations are added in quadrature. The upper and lower curves are defined as

$$D_{\rm max} = D_{\rm central} + \sqrt{(D_{\mu,\,\rm max} - D_{\rm central})^2 + (D_{m\,\rm max} - D_{\rm central})^2} \quad (1)$$

$$D_{\rm min} = D_{\rm central} + \sqrt{(D_{\mu,\,\rm min} - D_{\rm central})^2 + (D_{m\,\rm min} - D_{\rm central})^2} \quad (2)$$

where $D \equiv d\sigma/dp_T$ and the subscript 'central' is $m_c = 1.5$ GeV, $m_b = 4.75$ GeV with $\mu_F = \mu_R = \mu_0$, $D_{\mu,\,\rm max}$ is the maximum cross section obtained from the central mass value used with the scale ratios in our seven fiducial sets, and $D_{m\,\rm max}$ is the maximum cross section obtained from the mass variation with $\mu_R = \mu_F = \mu_0$. In Figs. 2 and 3, we compare the FONLL and the NLO charm and bottom p_T distributions. The results of the two methods are quite similar. At intermediate p_T, the FONLL result is somewhat larger while at higher p_T, where the NLO calculation includes large logs of p_T/m, the NLO result is somewhat larger. Both calculations lead to fairly similar values of the total cross section with the FONLL result being somewhat higher than the NLO result

The fragmentation functions $D(c \to D)$ and $D(b \to B)$, where D and B indicate a generic admixture of charm and bottom hadrons, are consistently extracted from e^+e^- data. The charm fragmentation function depends on the parameter r with $r = 0.1$ for $m_c = 1.5$ GeV, 0.135 for $m_c = 1.7$ GeV, and 0.06 for $m_c = 1.3$ GeV. Bottom fragmentation depends instead on the parameter α where $\alpha = 29.1$ for $m_b = 4.75$ GeV, 34 for $m_b = 5$ GeV, and 25.6 for $m_b = 4.5$ GeV. Fragmentation is numerically performed by rescaling the quark three-momentum at a constant angle in the laboratory frame.

Due to the fairly hard fragmentation function, the D meson and c quark distributions begin to differ outside the uncertainty bands only for $p_T > 9$ GeV, as seen on the left-hand side of Fig. 2. Note that the width of the uncertainty band is largest for low p_T where the scales are lowest and the scale sensitivity is thus greatest. The same comparison for bottom quarks and the subsequent B mesons shows that, as a result of the harder $b \to B$ fragmentation function, the two bands partially overlap for $p_T \simeq 20$ GeV and beyond, as seen on the right-hand side of Fig. 2. The quark and meson results are compared in the central rapidity region, $|y| < 0.75$. At forward rapidities, the shapes of the distributions are similar except at

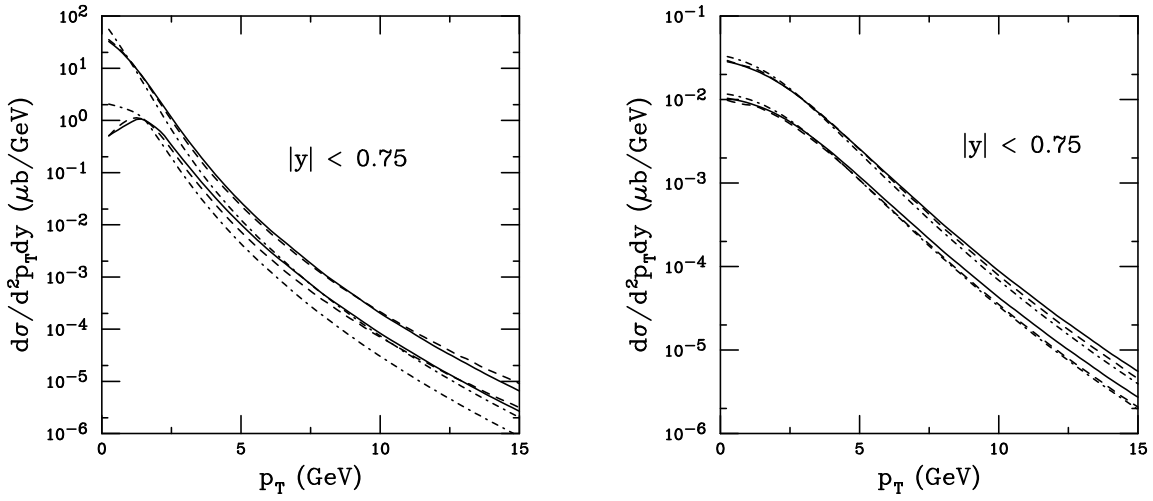

Fig. 2: The heavy quark theoretical band as a function of p_T for FONLL (solid curves) and NLO (dashed curves) in $\sqrt{s} = 200$ GeV pp collisions in the rapidity range $|y| \leq 0.75$. Also shown is the heavy flavor meson uncertainty band, all using the CTEQ6M parton densities. The left-hand plot gives the c quark and D meson results while the right-hand plot shows the b quark and B meson results.

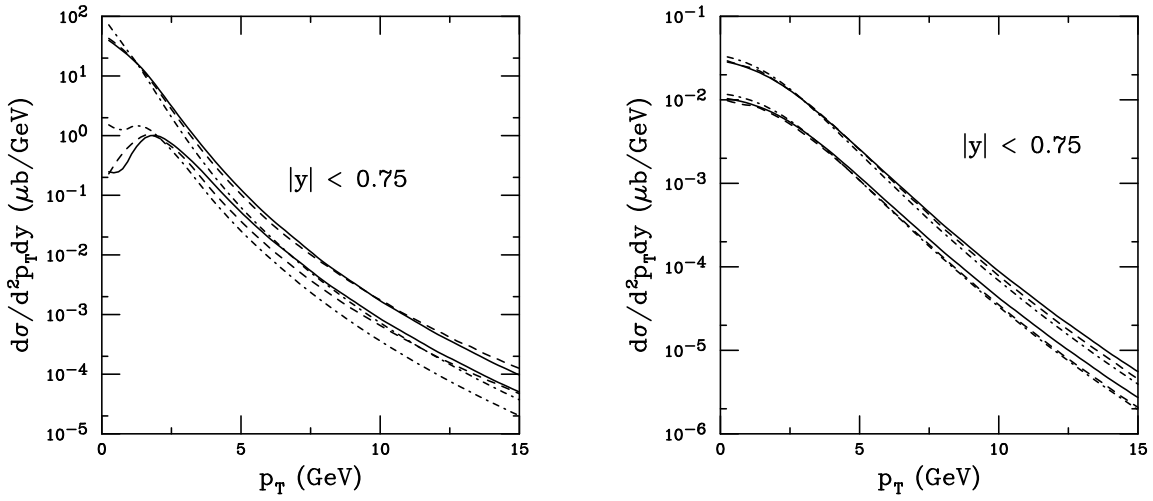

Fig. 3: The heavy quark theoretical band as a function of p_T for FONLL (solid curves) and NLO (dashed curves) in $\sqrt{s} = 500$ GeV pp collisions in the rapidity range $|y| \leq 0.75$. Also shown is the heavy flavor meson uncertainty band, all using the CTEQ6M parton densities. The left-hand plot gives the c quark and D meson results while the right-hand plot shows the b quark and B meson results.

low p_T where the charm p_T uncertainty band is somewhat narrower since both x_1 and x_2 in the gluon densities are not simultaneously small. Since the results are otherwise similar, the forward curves are not shown here. We give the 500 GeV charm and bottom predictions in Fig. 3. In general, the higher energy leads to harder p_T distributions.

The calculation of quarkonium cross sections in the color evaporation model is described in Ref. [2]. We have included intrinsic transverse momentum, k_T, to broaden the quarkonium p_T distributions. In the NLO code, the k_T kick is applied in the final state according to a Gaussian distribution, assuming that the x and k_T dependencies in the parton densities factorizes. In this case, it then does not matter whether the k_T is applied in the initial or final state.

In NLO the code, the $Q\overline{Q}$ system is boosted to rest from its longitudinal center of mass frame. Transverse momenta of the incoming partons, $\vec{k}_{T1}$ and $\vec{k}_{T2}$, are chosen at random. A second transverse boost out of the pair rest frame changes the initial transverse momentum of the $Q\overline{Q}$ pair, $\vec{p}\,'_T$, to $\vec{p}\,'_T+\vec{k}_{T1}+\vec{k}_{T2}$. The initial k_T of the partons could have alternatively been given to the entire final-state system, as is essentially done if applied in the initial state, instead of to the $Q\overline{Q}$ pair. There is no difference if the calculation is to LO only but at NLO an additional light parton also appears in the final state. The difference in the two methods is rather small if $k_T^2 \leq 2$ GeV^2. The effect of the intrinsic k_T decreases as $\sqrt{s}$ increases since the average of p_T distribution, before the k_T broadening is applied, increases with energy.

We have compared the p_T distributions with broadening to the Tevatron Run I quarkonium results. We found that a $\langle k_T^2 \rangle$ value of 2.5 GeV^2 is needed to sufficiently broaden the calculated distributions, higher than that determined from lower energy charm production data. A simple logarithmic dependence on the energy,

$$\langle k_T^2 \rangle_p = 1 + \frac{1}{6} \ln \left(\frac{S}{S_0} \right) \text{ GeV}^2 \ , \tag{3}$$

with $\sqrt{S_0} = 20$ GeV, can account for the increase. Thus for $\sqrt{S} = 200$ and 500 GeV, $\langle k_T^2 \rangle_p = 1.77$ GeV^2 and 2.07 GeV^2 respectively. The k_T broadening due to the presence of nuclear matter is applied as in Ref. [3]. Sample J/ψ and Υ p_T distributions in 200 GeV pp and p+Au collisions and 500 GeV pp collisions at RHIC are shown in Figs. 4 and 5 respectively in the central region, $|y| \leq 0.75$ and the forward region $1.2 < y < 2.2$. There is little effect of broadening seen in pA with respect to pp collisions. In addition, the effects of initial state shadowing, included using the EKS98 parameterization, cannot be discerned on the logarithmic scale of the p_T distributions except perhaps at low p_T in the forward region. For a complete discussion of the effects of shadowing and nucleon absorption in d+Au collisions at RHIC as a function of rapidity, see Ref. [4].

References

[1] M. Cacciari, P. Nason and R. Vogt, hep-ph/0502203.

[2] M. Bedjidian *et al.*, hep-ph/0311048.

[3] R. Vogt, Int. J. Mod. Phys. **E12** (2003) 211.

[4] R. Vogt, hep-ph/0411378, Phys. Rev. C, in press.

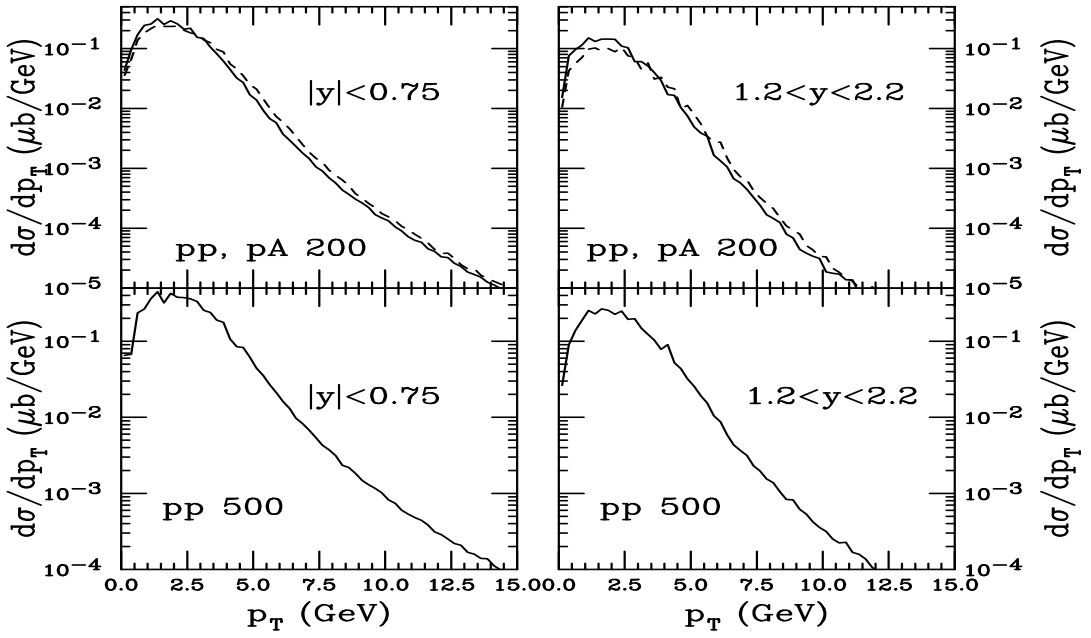

Fig. 4: The inclusive J/ψ p_T distributions at $\sqrt{s} = 200$ and 500 GeV using case $\psi 1$ (solid). We use $\langle k_T^2 \rangle_p = 1.77$ GeV^2 for pp collisions and include broadening in pA collisions (dashed).

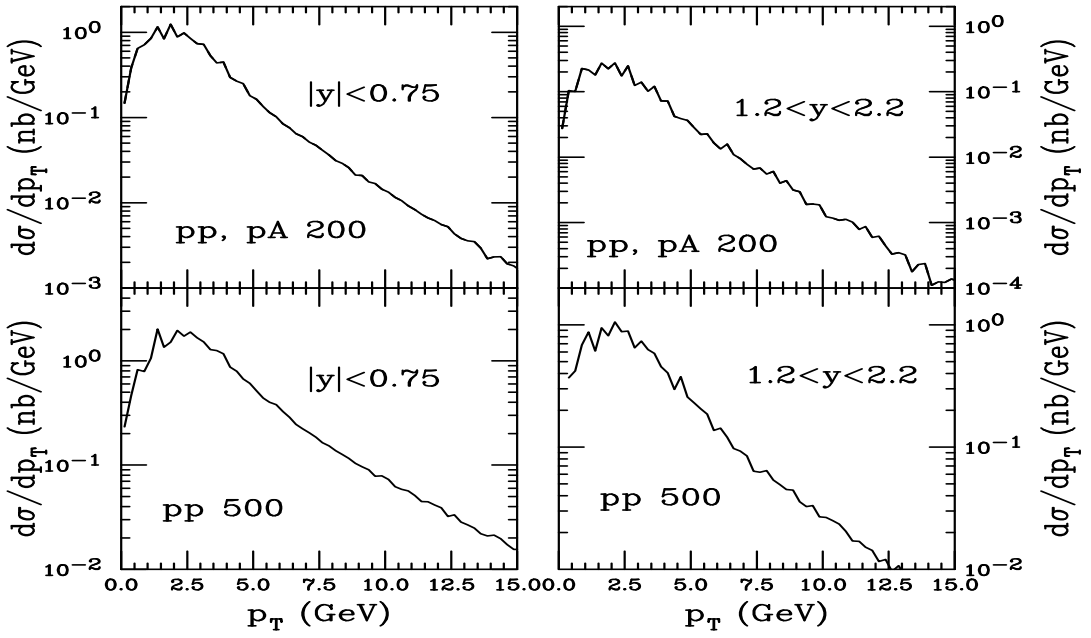

Fig. 5: The inclusive Υ p_T distributions at $\sqrt{s} = 200$ and 500 GeV using case $\Upsilon 1$. We use $\langle k_T^2 \rangle_p = 1.77$ GeV^2 for pp collisions.